Modeling and Control of Ultracold Atoms Trapped in an Optical Lattice

AN EXAMPLE-DRIVEN TUTORIAL ON QUANTUM CONTROL

MARCO M. NICOTRA, JIEQIU SHAO, JOSHUA COMBES, ANNE CROSS THEURKAUF, PENINA AXELRAD, LIANG-YING CHIH, MURRAY HOLLAND, ALEX A. ZOZULYA, CATIE K. LEDESMA, KENDALL MEHLING, and DANA Z. ANDERSON

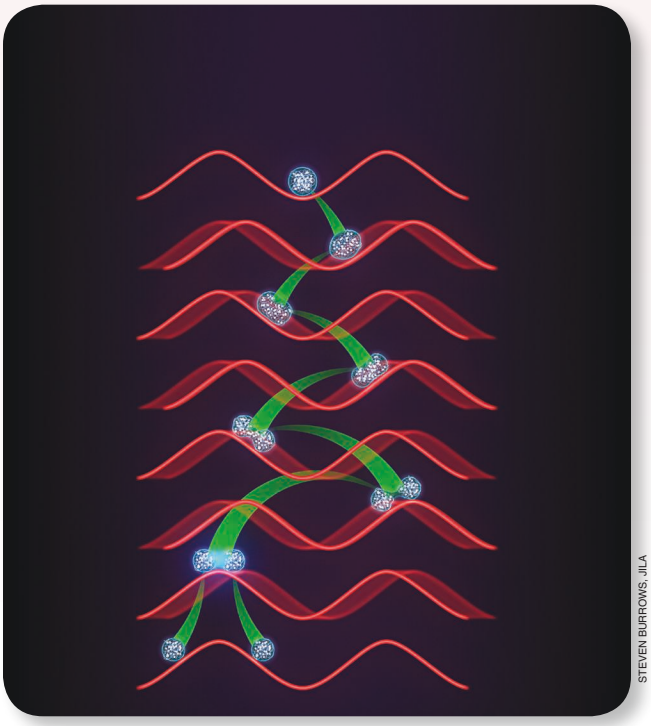

STEVEN BURROWS, JILA

The laws of quantum mechanics capture the behavior of physical systems at the smallest observable spatiotemporal scales. By pushing systems to the very edge of physical limits, quantum technology has the potential to revolutionize the state of the art in a variety of domains, including metrology [1], [2], [3], [4], communication [5], [6], [7], and computing [8], [9], [10]. As the field continues its transition from a scientific curiosity to an engineering endeavor, experimental prototypes found in physics laboratories must be converted into reliable hardware platforms that operate in less sheltered contexts. This step (from quantum science to quantum engineering) represents a unique opportunity for the IEEE Control Systems Society to provide meaningful insights on how to systematically steer these systems to the desired operating point.

The aim of this article is to familiarize the reader with quantum control by describing a physically relevant application [transitioning a Bose–Einstein condensate (BEC) from its lowest energy state to its first excited state] from the perspective of a classical control engineer. The article makes no assumptions on the audience beyond a basic knowledge of linear algebra, complex numbers, and differential equations. See also "Summary." Specifically, we will 1) provide a step-by-step derivation of the dynamic model, 2) analyze the autonomous system to identify meaningful control objectives, 3) introduce a selection of quantum control strategies for achieving said objectives, and 4) compare the closed-loop behavior obtained with each strategy. This application-driven tutorial complements existing literature surveys [11], [12], [13] that feature a more comprehensive overview of quantum control theory in the general setting. For the reader's convenience, "An Introduction to Dirac Notation" briefly introduces the conventional notation used in quantum literature, whereas "An Introduction to Quantum Mechanics" provides an overview of the fundamental mathematical postulates that describe quantum physics.

Digital Object Identifier 10.1109/MCS.2022.3216652
Date of current version: 9 January 2023

1066-033X/23©2023IEEE

A DYNAMIC MODEL OF TRAPPED ULTRACOLD ATOMS

When a gas of identical atoms is cooled close to 0 K, the atoms "condense" into a spatially localized region and collectively behave as a new entity called a *BEC,* which is a fifth phase of matter. An interesting property of BECs (also known as *ultracold atoms*) is that they exhibit quantum mechanical behaviors at a macroscopic scale ($\approx 200\ \mu$m). To

Summary

This article is the product of a three-year multidisciplinary collaboration between a team of control engineers and a team of quantum scientists. In the author's experience, the greatest challenge one faces when entering the field of quantum control is the language barrier between the two communities. The aim of this article is to lower this barrier by showing how familiar control strategies (that is, Lyapunov, optimal control, and learning) can be applied in the unfamiliar setting of a quantum system (that is, a cloud of trapped ultracold atoms). Particular emphasis is given to the derivation of the model and the description of its structural properties. Sidebars throughout the article prove a brief overview of the essential notions/notation required to establish an effective communication channel with quantum physicists and quantum engineers. In essence, this article is a collection of everything that our control team wished they had known at the beginning of the project. It is our hope that it may be of assistance to members of this community wanting to embark on their first quantum control project.

An Introduction to Dirac Notation

The Dirac (or *"bra–ket"*) notation [S1] is pervasive to modern physics literature and is used to denote linear algebraic operations in Hilbert space, which is a complete vector space that admits an inner product operator $\langle \cdot | \cdot \rangle$. Although this sidebar focuses on finite-dimensional spaces for ease of exposition, the general intuition can be readily extended to infinite-dimensional spaces, as detailed in [S2] and [S3]. Elements of a Hilbert space $\mathcal{H}$ are identified using the *"ket"* operator $|\psi\rangle \in \mathcal{H}$. Conversely, the *"bra"* operator $\langle \psi | \in \mathcal{H}^\dagger$ identifies elements of the inner product-induced dual space $\mathcal{H}^\dagger$. Thus, the inner product $\langle \cdot | \cdot \rangle$ can be reduced to a simple multiplication between a bra $\langle \cdot |$ and a ket $| \cdot \rangle$. If we consider the space of complex column vectors, for example, the inner product is defined as $\langle \phi | \psi \rangle = \phi^\dagger \psi$, where $\phi^\dagger$ is the complex conjugate transpose of ϕ. In Dirac notation, $|\psi\rangle \in \mathcal{H}$ is a complex column vector, and $\langle \phi | \in \mathcal{H}^\dagger$ is a complex row vector satisfying $\langle \phi | = |\phi\rangle^\dagger$. If $\mathcal{H}$ is finite dimensional, the ket can be expressed as

$$|\psi\rangle = \sum_{n=1}^{N} \psi_n |e_n\rangle \tag{S1}$$

where ψ_n are complex numbers, and $|e_n\rangle$ are elements of an orthonormal basis of $\mathcal{H}$, meaning that they satisfy $\langle e_n | e_n \rangle = 1, \forall n$, and $\langle e_m | e_n \rangle = 0, \forall m \neq n$. Similarly, the bra can be expressed as

$$\langle \phi | = \sum_{n=1}^{N} \phi_n^* \langle e_n | \tag{S2}$$

where ϕ_n^* is the complex conjugate of ϕ_n. Following from (S1) and (S2) and the properties of an orthonormal basis, the inner product reduces to $\langle \phi | \psi \rangle = \Sigma_{n=1}^{N} \phi_n^* \psi_n$, which satisfies the noncommutative property $\langle \psi | \phi \rangle = (\langle \phi | \psi \rangle)^*$. Finally, $|\psi\rangle \in \mathcal{H}$ is unitary if $\langle \psi | \psi \rangle = 1$. Elements in Hilbert space can be manipulated by operators in the form $A : \mathcal{H} \to \mathcal{H}$. Operators A and B are linear if and only if

- $A | \psi \rangle = | A\psi \rangle, \quad \forall | \psi \rangle \in \mathcal{H};$
- $(A + B) | \psi \rangle = A | \psi \rangle + B | \psi \rangle, \quad \forall | \psi \rangle \in \mathcal{H};$
- $A(\alpha | \psi \rangle + \beta |\phi\rangle) = \alpha A|\psi\rangle + \beta A|\phi\rangle, \quad \forall |\psi\rangle, |\phi\rangle \in \mathcal{H}, \forall \alpha, \beta \in \mathbb{C}.$

Given a linear operator A, $\lambda_\nu \in \mathbb{C}$ and $| \nu \rangle \in \mathcal{H}$ are, respectively, an eigenvalue and an eigenvector of A if they satisfy the property $A | \nu \rangle = \lambda_\nu | \nu \rangle$. Given a linear operator A, its Hermitian adjoint $A^\dagger$ is such that $\langle A\psi | = \langle \psi | A^\dagger$. Combined with the noncommutative property of the inner product, the Hermitian adjoint satisfies $\langle \psi | A | \phi \rangle = (\langle \phi | A^\dagger | \psi \rangle)^*$. An operator A is *Hermitian*, that is, it satisfies $A = A^\dagger$, only if all of its eigenvalues are real. Operators can be constructed as the outer product of a bra and a ket, that is, $| \cdot \rangle\langle \cdot |$. Notable examples include the *identity operator* $I = \Sigma_{n=1}^{N} | e_n \rangle\langle e_n |$ and the *projection operator*

$$\Pi_\psi = |\psi\rangle\langle\psi| \tag{S3}$$

which can be used to compute the following:

- *Projection*: $\Pi_\psi | \phi \rangle$ denotes the projection of $| \phi \rangle$ onto the unit vector $| \psi \rangle$. Note that $(\langle \psi | \phi \rangle) | \psi \rangle = | \psi \rangle (\langle \psi | \phi \rangle) = | \psi \rangle\langle \psi \| \phi \rangle = \Pi_\psi | \phi \rangle$.
- *Inner product, squared*: $\langle \phi | \Pi_\psi | \phi \rangle$ denotes the modulus square of the inner product $\langle \psi | \phi \rangle$. Note that $|\langle \psi | \phi \rangle|^2 = (\langle \psi | \phi \rangle)^* \langle \psi | \phi \rangle = \langle \phi | \psi \rangle \langle \psi | \phi \rangle = \langle \phi | \Pi_\psi | \phi \rangle$.
- *Hilbert–Schmidt distance, squared*: $\langle \phi | (I - \Pi_\psi) | \phi \rangle$ denotes the squared distance between the unit vectors $| \phi \rangle$ and $| \psi \rangle$. Note that $1 - |\langle \psi | \phi \rangle|^2 = \langle \phi | \phi \rangle - \langle \phi | \Pi_\psi | \phi \rangle = \langle \phi | (I - \Pi_\psi) | \phi \rangle$.

REFERENCES

[S1] P. Dirac, "A new notation for quantum mechanics," *Math. Proc. Cambridge Philos. Soc.*, vol. 35, no. 3, pp. 416–418, Jul. 1939, doi: 10.1017/S0305004100021162.

[S2] C. J. Isham, *Lectures on Quantum Theory: Mathematical and Structural Foundations*. London, U.K.: Imperial College Press, 1995.

[S3] F. Gieres, "Mathematical surprises and Dirac's formalism in quantum mechanics," *Rep. Prog. Phys.*, vol. 63, no. 12, p. 1893, Dec. 2000, doi: 10.1088/0034-4885/63/12/201.

manipulate BECs, it is convenient to "trap" them in a spatially confined region using two counterpropagating laser beams that create a standing wave known as an *optical lattice*. An experimental process for obtaining trapped BECs is described in "Obtaining a Bose–Einstein Condensate." The trapped BEC can then be controlled by changing the phase of (that is, *shaking*) the optical lattice. The ability to make BECs has enabled a variety of quantum science and technology applications, such as interferometry [14], [15], [16], [17], vortex production [18], [19], black hole simulation [20], [21], [22], and lithography [23], [24]. The dynamical model of a BEC can be obtained by specializing the Schrödinger equation [(S6) in "An Introduction to Quantum Mechanics"] to a cloud of trapped ultracold atoms. This is achieved by finding a suitable expression for the kinetic and potential energy operators. For simplicity, this article addresses a 1D model. As detailed in [25], the kinetic energy operator for a system expressed in a 1D position space $x \in \mathbb{R}$ is

$$K = -\frac{\hbar^2}{2m}\frac{\partial^2}{\partial x^2} \tag{1}$$

where m is the mass of the particle and $\hbar \approx 1.055 \cdot 10^{-34}$ Js is the reduced Planck constant. To obtain the potential energy operator, consider two counterpropagating laser beams of wavelength λ and phase θ. Their combined electromagnetic field is

$$E(x) = E_1 e^{i(kx+\theta)} + E_2 e^{-i(kx+\theta)} \tag{2}$$

where $k = 2\pi/\lambda$ is the wavenumber of the laser beams, and E_1 and E_2 are the amplitudes of each beam. The resulting electromagnetic intensity is

$$I(x) = E^* E = E_1^2 + E_2^2 + 2E_1 E_2 \cos(2kx + 2\theta). \tag{3}$$

Since the laser is usually tuned so that atoms are attracted to the regions of highest intensity, the minimum potential energy corresponds to x such that $\cos(2kx + 2\theta) = 1$, whereas the maximal potential energy is where $\cos(2kx + 2\theta) = -1$. Based on this intuition, the potential energy operator associated with the optical lattice is

$$U = -\frac{U_0}{2}\cos(2kx + u) \tag{4}$$

where U_0 is the optical depth (that is, the difference between the maximum and minimum potential), and $u = 2\theta$ is the phase of the optical lattice (which acts as a control input for the system). In practice, the optical depth U_0 can be measured experimentally using the procedure detailed in [26]. Thus, the Schrödinger equation [(S6) in "An Introduction to Quantum Mechanics"] specializes to

$$i\hbar\frac{\partial}{\partial t}\Psi(x,t) = -\frac{\hbar^2}{2m}\frac{\partial^2}{\partial x^2}\Psi(x,t) - \frac{U_0}{2}\cos(2kx + u)\Psi(x,t) \tag{5}$$

where $\Psi(x,t) \equiv \langle x \,|\, \Psi \rangle$ is a time-varying wave function represented in a 1D position space. "Momentum Basis Decomposition" details how this partial differential equation can be approximated as the ordinary differential equation (ODE)

An Introduction to Quantum Mechanics

Quantum theory describes the behavior and experimental observation of objects that are both very small and well isolated (for example, particles). Such objects are said to be "quantized" if one or more of their observable properties (for example, energy) are fundamentally discrete. The complete framework of quantum theory emerges from a few mathematical postulates:

1) *Wave function*: The state of an isolated quantum object is fully described by a wave function $|\Psi\rangle \in \mathcal{H}$, with $\langle \Psi | \Psi \rangle = 1$.
2) *Observables*: All observable properties of the object are associated to a Hermitian operator. Notable examples include position, momentum, kinetic energy, and potential energy.
3) *Measurements*: When measuring an observable A, the measurement outcome can only be one of its eigenvalues λ_n. The probability of obtaining a specific outcome λ_n is

$$P(\lambda_n) = \langle \Psi | \Pi_n | \Psi \rangle \tag{S4}$$

where $\Pi_n = |n\rangle\langle n|$ is the projection onto the eigenvector $|n\rangle$ associated to λ_n. In other words, the likelihood of measuring a given eigenvalue of the observable is proportional to how much the wave function is aligned with the corresponding eigenvector. Moreover, the state after the measurement becomes

$$|\Psi'\rangle = \frac{\Pi_n |\Psi\rangle}{\sqrt{P(\lambda_n)}}. \tag{S5}$$

This phenomenon is known as "wave function collapse."

4) *Schrödinger equation*: The dynamic behavior of the wave function is governed by the complex partial differential equation

$$i\hbar\frac{\partial}{\partial t}|\Psi\rangle = H|\Psi\rangle \tag{S6}$$

where $H = K + U$ is the Hamiltonian operator, K is the kinetic energy operator, U is the potential energy operator, i is the imaginary unit, and $\hbar \approx 1.055 \cdot 10^{-34}$ Js is the reduced Planck constant.

Although this prescription of quantum theory is sufficient for the purpose of this article, it should be noted that each postulate admits a more general formulation. Readers interested in a more thorough description of quantum theory are referred to [25] and [S2].

Obtaining a Bose–Einstein Condensate

What is observed as "temperature" is a physical quantity related to the amount of energy stored in degrees of freedom, such as rotation, vibration, and speed of atoms. At 0 K (that is, absolute zero), the atoms would have no energy. To condense a cloud of atoms into a Bose–Einstein condensate (BEC), the ensemble must typically be cooled down to a critical temperature of around 100 nK so that their motional velocity is in the millimeter/second range. This multistage process is performed in a glass cell held under ultrahigh vacuum, as illustrated in Figure S1.

DOPPLER COOLING

The initial cooling step consists in irradiating the atomic gas with three pairs of mutually perpendicular counterpropagating laser beams of properly selected polarization and frequency.

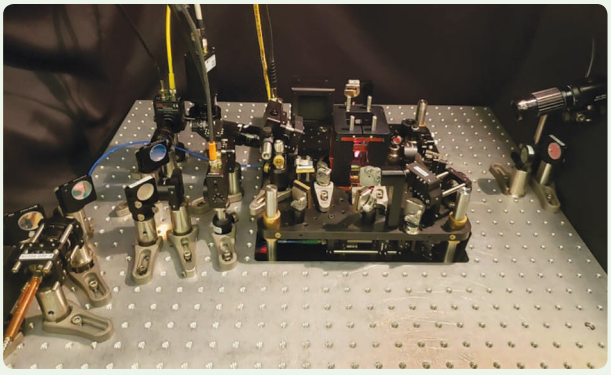

FIGURE S1 The experimental setup used to obtain the Bose–Einstein condensate.

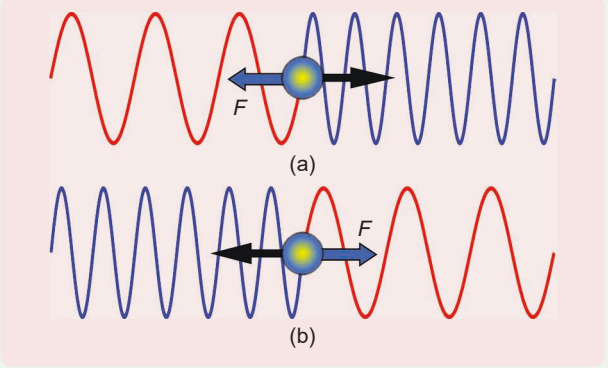

FIGURE S2 An illustration of the Doppler cooling effect for atoms moving (a) to the right and (b) to the left. Because of the Doppler effect, atoms experience a blue-shifted frequency in the direction they are traveling toward. Since the laser frequency is only slightly detuned with respect to atomic resonance, this Doppler shift is sufficient to trigger the absorption of photons from the blue-shifted laser beam. Because of the conservation of momentum, the absorption of a photon causes the atom to slow down, thereby resulting in a damping force F that always opposes movement.

Here, the laser frequency is slightly detuned below atomic resonance (that is, the frequency at which the atoms would absorb photons from the laser beam). Due to the Doppler effect, illustrated in Figure S2, atoms moving toward an incoming laser beam experience a slight frequency shift that triggers photon absorption. By shining in light from all six directions, a laser force always opposes the direction of the atom's motion, causing a reduction of the atom's speed and, therefore, its temperature. Trapping is then accomplished via magnetic fields whose gradients, combined with the applied laser, introduce the necessary forces to contain atoms in the center of the cell. This is known as a magneto-optical trap (MOT), which can capture roughly 10^9 atoms at $\approx 300\ \mu$K. Figure S3 features an experimental picture of a MOT.

POLARIZATION GRADIENT COOLING

Atoms are further cooled by spatially compressing the MOT and detuning the laser light frequency to perform polarization gradient cooling. This reduces the temperature of the trapped atoms to $\approx 20\ \mu$K.

EVAPORATION COOLING

To cool down to the nanokelvin regime where a BEC is formed, the atoms must undergo a final stage known as evaporative

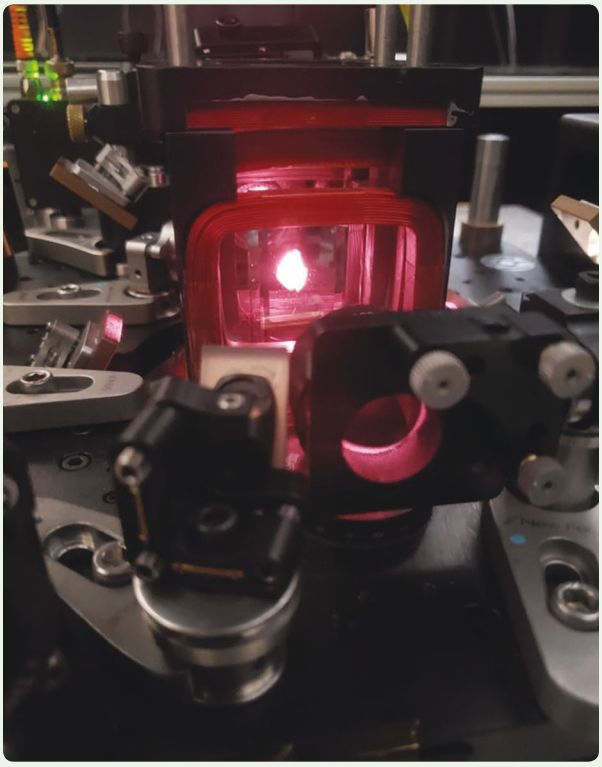

FIGURE S3 A close-up of a cloud of atoms contained in the magneto-optical trap. The size of the cloud is ≈ 4 mm.

(*Continued*)

Obtaining a Bose–Einstein Condensate (*Continued*)

cooling. This consists of transferring the atoms into a potential well—either magnetic or optical—and slowly lowering the walls of the trap potential, as illustrated in Figure S4. As the walls are lowered, hotter atoms are allowed to escape, and the remaining atoms rethermalize to colder temperatures. This is repeated until a BEC is achieved at ≈ 300 nK, with the formation of the condensate being quite sudden (like supercooled water turning to ice). Figure S5 features experimental data of a BEC measurement.

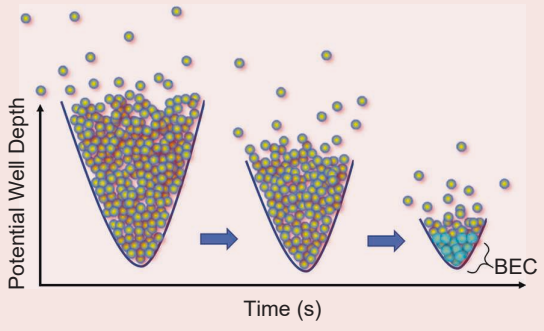

FIGURE S4 Once atoms are loaded into a potential well, the well depth is slowly ramped down over time. As this occurs, the hotter atoms leave the trap, and the remaining atoms rethermalize and become colder (the same way hot coffee is cooled down by the evaporation of steam). Eventually, when the trap is shallow enough, some of the remaining atoms will become cold enough to condense into a Bose–Einstein condensate (BEC). These atoms are shown in cyan.

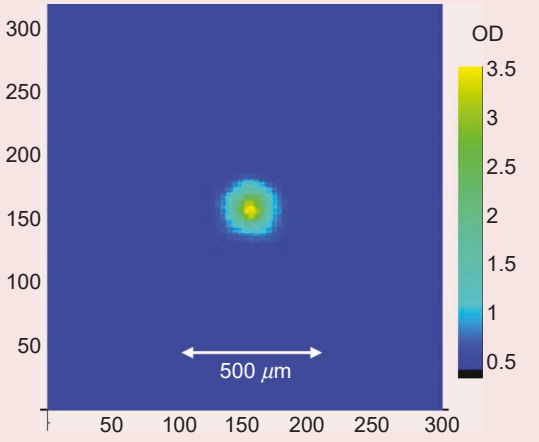

FIGURE S5 An absorption image of a typical Bose–Einstein condensate containing approximately 70k atoms. Absorption imaging is done by shining resonant light on the atoms, which is absorbed, and taking the natural log of the difference between that and a background image containing no atoms. The optical density (OD) is a measure of the number of atoms in the image. Both the *x*- and *y*-axes depict the pixel number in camera coordinates.

$$i|\dot{\psi}\rangle = H_0|\psi\rangle + \sin(u)H_1|\psi\rangle + (\cos(u)-1)H_2|\psi\rangle \tag{6}$$

where $|\psi\rangle$ is a quantum state, which can be represented as a time-varying complex column vector, and H_0, H_1, and H_2 are the Hermitian matrices given in (S10) of "Momentum Basis Decomposition." To further simplify the system, it is customary to introduce the small-angle approximation (that is, $\sin u \approx u$ and $\cos u \approx 1$) and reduce (6) to the bilinear model

$$i|\dot{\psi}\rangle = H_0|\psi\rangle + uH_1|\psi\rangle. \tag{7}$$

"Eigenstates of the Hamiltonian" addresses, among other things, the validity of the ODE approximation (6). The validity of the bilinear approximation (7) is instead discussed in the section "Optimal Control."

SYSTEM ANALYSIS

This section analyzes the structural properties of (6) and (7) to identify what can and cannot be achieved through the use of control. We first show that the wave function $|\psi\rangle$ can only evolve on the unit sphere (readers familiar with rigid body attitude control will recognize that this behavior is analogous to that of unit quaternions [27]). We then prove that our system does not admit any equilibrium points on the unit sphere, and that the only invariant sets of the system are actually periodic orbits. As detailed in [25], $|\psi\rangle \in \mathbb{C}^{2N+1}$ is a wave function only if $\langle\psi(t)|\psi(t)\rangle = 1, \forall t$. It is therefore reasonable to expect that the unitary sphere $\mathbb{S} = \{|\psi\rangle \in \mathbb{C}^{2N+1} | \langle\psi|\psi\rangle = 1\}$ is an invariant manifold. To verify this property under the generalized Schrödinger equation $i|\dot{\psi}\rangle = H(u)|\psi\rangle$, we show that

$$\begin{aligned}\frac{\partial}{\partial t}\langle\psi|\psi\rangle &= \langle\dot{\psi}|\psi\rangle + \langle\psi|\dot{\psi}\rangle \\ &= \langle -iH(u)\psi|\psi\rangle + \langle\psi|-iH(u)\psi\rangle \\ &= \langle\psi|i(H(u)^\dagger - H(u))|\psi\rangle.\end{aligned}$$

Since $(\partial/\partial t)\langle\psi|\psi\rangle = 0$ if and only if $H(u)^\dagger = H(u), \forall u$, the unit sphere $\mathbb{S}$ is invariant if and only if $H(u)$ is Hermitian. Given $H(u) = H_0 + \sin(u)H_1 + (\cos(u)-1)H_2$ in the nonlinear case (6) and $H(u) = H_0 + uH_1$ in the bilinear case (7), the invariance of $\mathbb{S}$ follows directly from (S10) (which defines H_0, H_1, and H_2 as Hermitian matrices). Having proven that $|\psi(t)\rangle$ evolves on the unit sphere, we aim to characterize the system's behavior in the absence of a control input. Specifically, given

$u(t) = 0$, both (6) and (7) reduce to the same autonomous system

$$i|\dot{\psi}\rangle = H_0|\psi\rangle. \tag{8}$$

Whenever $\text{null}(H_0) = 0$ [which is the case for (S10)], the system does not admit any equilibrium points in $\mathbb{S}$. As such, the traditional control objective *"Design u(t) such that $\tilde{x}$ is a globally asymptotically stable equilibrium point"* may not

Momentum Basis Decomposition

Since the potential energy operator (4) is periodic, it follows from the Bloch theorem ([S4], Chapter 7) that the position space representation of the wave function $|\Psi\rangle$ can be written as a linear combination of periodic functions. As a result,

$$\Psi(x,t) = \langle x|\Psi\rangle = \sum_{n=-\infty}^{\infty} \psi_n(t) e^{i2nkx} \tag{S7}$$

where $\psi_n(t)$ are time-dependent complex-valued scalars. Substituting (S7) into the Schrödinger equation (5) and omitting the dependency on t to simplify the notation leads to

$$i\hbar \sum_{n=-\infty}^{\infty} \dot{\psi}_n e^{i2nkx} = \sum_{n=-\infty}^{\infty} -\frac{\hbar^2}{2m}\psi_n \nabla_x^2 e^{i2nkx} - \frac{U_0}{2}\cos(2kx+u)\,\psi_n e^{i2nkx}.$$

Noting that

$$\nabla_x^2 e^{i2nkx} = -(2nk)^2 e^{i2nkx}$$

and

$$\cos(2kx+u)e^{i2nkx} = \frac{e^{i2kx}e^{iu} + e^{-i2kx}e^{-iu}}{2} e^{i2nkx} = \frac{e^{iu}}{2} e^{i2(n+1)kx} + \frac{e^{-iu}}{2} e^{i2(n-1)kx}$$

it is possible to rewrite the Schrödinger equation (5) as

$$i\hbar \sum_{n=-\infty}^{\infty} \dot{\psi}_n e^{i2nkx} = \sum_{n=-\infty}^{\infty} \left(\frac{\hbar^2}{2m}(2nk)^2 \psi_n - \frac{U_0}{4}\left(\psi_{n-1}e^{iu} + \psi_{n+1}e^{-iu}\right)\right) e^{i2nkx}.$$

By grouping the coefficients of each basis function e^{i2nkx}, the Schrödinger equation can then be reformulated in terms of the individual wave function coefficients $\psi_n(t)$, which are subject to the dynamics

$$i\hbar\dot{\psi}_n = E_R \begin{bmatrix} -\frac{\alpha}{4}e^{iu} & 4n^2 & -\frac{\alpha}{4}e^{-iu} \end{bmatrix} \begin{bmatrix} \psi_{n-1} \\ \psi_n \\ \psi_{n+1} \end{bmatrix} \tag{S8}$$

where $E_R = \hbar^2 k^2/2m$ is the recoil energy of the trapped particle, and $\alpha = U_0/E_R$ is the normalized lattice potential. To obtain a finite ordinary differential equation (ODE), consider the truncated vector of coefficients

$$\begin{bmatrix} \psi_{-N}(t) \\ \psi_{1-N}(t) \\ \vdots \\ \psi_{-1}(t) \\ \psi_0(t) \\ \psi_1(t) \\ \vdots \\ \psi_{N-1}(t) \\ \psi_N(t) \end{bmatrix} \tag{S9}$$

which belongs to the Hilbert space of complex column vectors and can thus be defined as a wave function in its own right if $\langle\psi(t)|\psi(t)\rangle = 1, \forall t$. To ensure that the vector in (S9) is a good representation of the full wave function in (S7), it is necessary to introduce (and verify) the assumption $\psi_n(t) \approx 0, \ \forall t \geq 0, \ \forall\, |n| > N$. Noting that $e^{\pm iu} = 1 \pm i\sin(u) + (\cos(u) - 1)$, the truncated version of the infinite-dimensional ODE (S8) can finally be rewritten as the finite ODE (7), with

$$H_0 = \omega_R \begin{bmatrix} 4N^2 & -\frac{\alpha}{4} & & & & & & & \\ -\frac{\alpha}{4} & 4(N-1)^2 & -\frac{\alpha}{4} & & & & & & \\ & \ddots & \ddots & \ddots & & & & & \\ & & -\frac{\alpha}{4} & 4 & -\frac{\alpha}{4} & & & & \\ & & & -\frac{\alpha}{4} & 0 & -\frac{\alpha}{4} & & & \\ & & & & -\frac{\alpha}{4} & 4 & -\frac{\alpha}{4} & & \\ & & & & & \ddots & \ddots & \ddots & \\ & & & & & & -\frac{\alpha}{4} & 4(N-1)^2 & -\frac{\alpha}{4} \\ & & & & & & & -\frac{\alpha}{4} & 4N^2 \end{bmatrix} \tag{S10}$$

$$H_1 = \omega_R \begin{bmatrix} 0 & i\frac{\alpha}{4} & & & & \\ -i\frac{\alpha}{4} & 0 & i\frac{\alpha}{4} & & & \\ & \ddots & \ddots & \ddots & & \\ & & -i\frac{\alpha}{4} & 0 & i\frac{\alpha}{4} & \\ & & & -i\frac{\alpha}{4} & 0 & \\ & & & & & \end{bmatrix}$$

$$H_2 = \omega_R \begin{bmatrix} 0 & -\frac{\alpha}{4} & & & & \\ -\frac{\alpha}{4} & 0 & -\frac{\alpha}{4} & & & \\ & \ddots & \ddots & \ddots & & \\ & & -\frac{\alpha}{4} & 0 & -\frac{\alpha}{4} & \\ & & & -\frac{\alpha}{4} & 0 & \\ & & & & & \end{bmatrix} \tag{S11}$$

where $\omega_R = E_R/\hbar$ is the recoil frequency of the trapped particle.

REFERENCE

[S4] C. Kittel, *Introduction to Solid State Physics*, 7th ed. New York, NY, USA: Wiley, 1996.

Eigenstates of the Hamiltonian

An interesting property of periodic potentials is that the associated eigenstates are described by alternating odd and even functions [S4]. Given the wave function $|\Psi\rangle$ featured in the original Schrödinger equation (5), in "Momentum Basis Decomposition," we computed an approximate wave function $|\psi\rangle$ by collecting the $2N+1$ coefficients of (S7) into a complex column

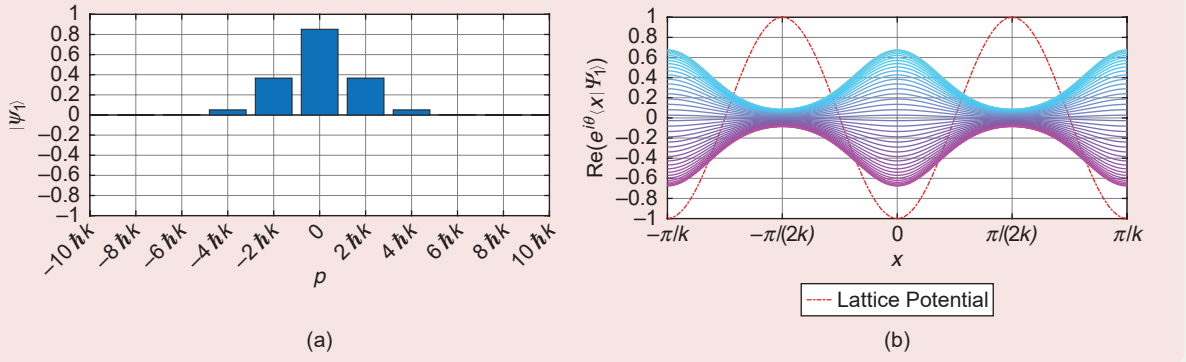

FIGURE S6 The first eigenstate of the Hamiltonian in (a) momentum space and (b) position space. In the momentum space representation, most of the atoms have a momentum of $p=0$ and are, therefore, stationary. In the position space representation, each curve represents the real part of the wave function evaluated at a different angle along the periodic orbit, starting from $\theta=0$ (cyan) to $\theta=\pi$ (magenta). Most of the atoms can be found in the wells of the lattice potential.

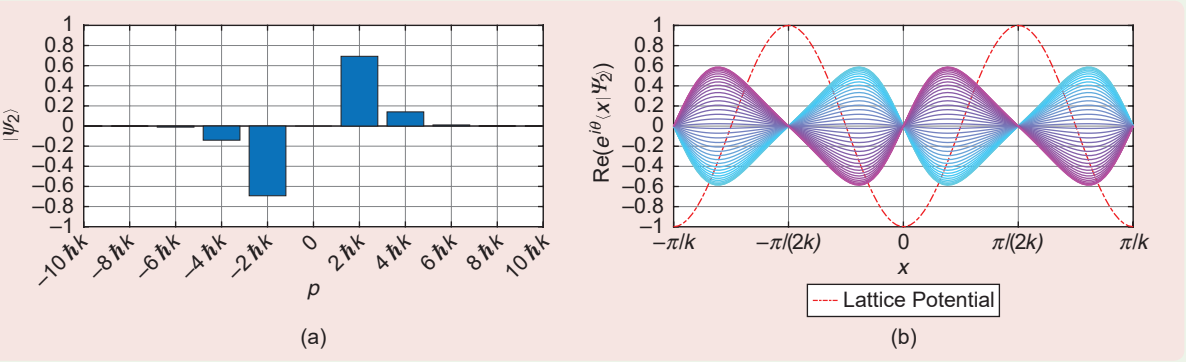

FIGURE S7 The second eigenstate of the Hamiltonian in (a) momentum space and (b) position space. In the momentum space representation, most of the atoms have a momentum of $p=\pm 2\hbar k$, meaning that there are actually two clouds of atoms moving in opposite directions. In the position space representation, the wave function is evaluated starting from $\theta=-\pi/2$ (cyan) to $\theta=\pi/2$ (magenta). Most of the atoms can be found where the slope of the optical lattice is at its steepest.

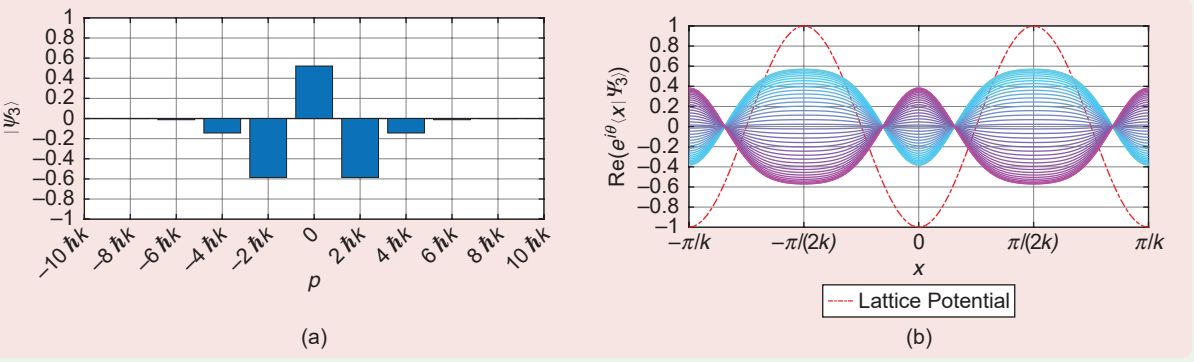

FIGURE S8 The third eigenstate of the Hamiltonian in (a) momentum space and (b) position space. In the momentum space representation, most of the atoms have a momentum of $p=\pm 2\hbar k$, but there is also a sizable portion with $p=0$. This describes a system with three clouds of atoms: two of which are moving in opposite directions, whereas one is standing still. In the position space representation, the wave function is evaluated starting from $\theta=0$ (cyan) to $\theta=\pi$ (magenta). Most of the atoms can be found at the peaks of the optical lattice potential, whereas a smaller portion is trapped in the wells.

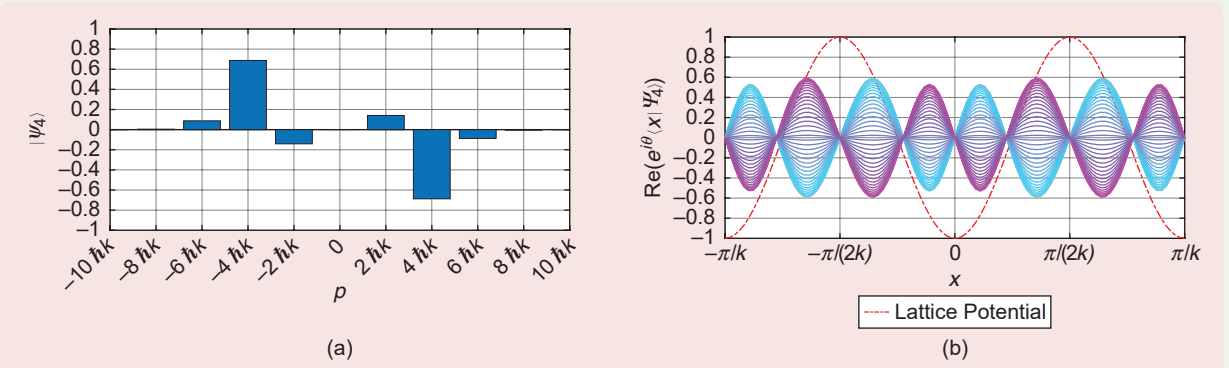

FIGURE S9 The fourth eigenstate of the Hamiltonian in (a) momentum space and (b) position space. In the momentum space representation, most of the atoms have a momentum of $p = \pm 4\hbar k$, meaning that there are once again two clouds of atoms moving in opposite directions, but they are separating at a faster rate than the second eigenstate. In the position space representation, the wave function is evaluated starting from $\theta = -\pi/2$ (cyan) to $\theta = \pi/2$ (magenta). The population is predominantly divided into four lobes within a single span of the lattice potential $x \in [-\pi/2k, \pi/2k]$.

vector $|\psi\rangle = [\psi_{-N} \ldots \psi_N]$, under the assumption that $\psi_n = 0$, $\forall\, |n| > N$. This led to the formulation of the approximate Hamiltonian H_0 in (S10). This sidebar studies the eigenvectors of H_0 to 1) verify the validity of the simplifying assumption and 2) provide a physical interpretation of what it means to go from one eigenstate to another. To provide some context, we introduce the notion of *momentum space*, which is a rescaled Fourier transform of the *position space*, that is,

$$\psi(p) = \frac{1}{\sqrt{2\pi\hbar}} \int_{-\infty}^{\infty} \Psi(x) e^{-ipx/\hbar} dx \tag{S12}$$

in a similar way to how the *frequency domain* is the Fourier transform of the *time domain*. The main difference is that (due to the scaling factor $\hbar$) the position and momentum pair is measured in meters and Joule seconds/meter, respectively, as opposed to the time and frequency pair (which is measured in seconds and 1/seconds, respectively) Equation (S7) can thus be interpreted as a "spatial frequency" decomposition of the wave function $|\Psi\rangle$, where each coefficient ψ_n represents the amplitude of a spatial sinusoid with momentum $\hbar \cdot (2nk)$. Figures S6–S9 illustrate the first four eigenstates of the system in both momentum space and position space. The momentum space representation is obtained simply by plotting the νth eigenvector of the Hamiltonian matrix H_0. The position space representation is then obtained by computing

$$\Psi_\nu(x) = \langle x | \Psi \rangle = \sum_{n=-N}^{N} \nu_n e^{i\,2nk\,x} \tag{S13}$$

and plotting the position representation $\mathrm{Re}(e^{i\theta}\Psi_\nu(x))$ for different values of θ to show how the wave function evolves along the periodic orbit O_ν. Based on these figures, we note the following emerging behavior:

Momentum space properties

- If ν is odd, the eigenvector is symmetric with respect to $p = 0$, and most of the population is in $p = \pm((\nu - 1)/2)(2\hbar k)$.
- If ν is even, the eigenvector is antisymmetric with respect to $p = 0$, and most of the population is in $p = \pm(\nu/2)(2\hbar k)$.

Position space properties

- Each eigenstate features ν lobes within the period $x \in [-(\pi/2k), \pi/2k]$.
- Odd-numbered eigenstates are symmetric with respect to $x = 0$, whereas even-numbered eigenstates are antisymmetric with respect to $x = 0$.

The validity of the ordinary differential equation (6) can therefore be verified a posteriori by checking whether or not a given numerical simulation excited the higher order modes

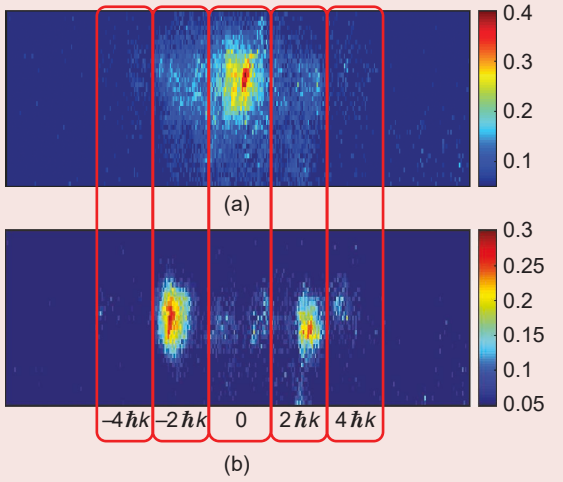

FIGURE S10 Experimental measurements of the (a) first and (b) second eigenstates of trapped ultracold atoms. These measurements were taken by turning off the optical lattice, waiting a set amount of time (that is, the *time of flight*), illuminating the atoms with a short pulse of resonant light, and then using a camera to acquire the shadows cast by the atoms. Turning off the laser causes the Bose–Einstein condensate to split into multiple clouds of atoms based on their momentum distribution, which enables turning a *momentum* measurement into a *position* measurement. The population (that is, $|\psi_n|^2$) of each momentum bin (that is, $2n\hbar k$) can then be computed by quantifying the optical intensities of each blob.

(*Continued*)

Eigenstates of the Hamiltonian (*Continued*)

of the system. This can be done by monitoring the value of $\langle\psi(t)|\Pi_N|\psi(t)\rangle$, where $\Pi_N = |N\rangle\langle N|$ is the projection onto the Nth eigenvector, and ensuring it stays under a set tolerance. A comparison of Figures S6 and S7 provides a physical interpretation of what it means to transition from the first eigenstate (also known as the *"ground state"*) to the second eigenstate. This transition takes a Bose–Einstein condensate (BEC) that is essentially at rest (which is the starting condition of a BEC obtained by bringing the atoms to a very low energy state) and separates it into two counterpropagating clouds of atoms with a momentum of $\pm 2\hbar k$. Similarly, the transition from the first to the fourth eigenstate means splitting the BEC into two counterpropagating clouds of atoms with a momentum of $\pm 4\hbar k$. Figure S10 features experimental measurements of the first and second eigenstates of a BEC trapped in an optical lattice.

be a well-posed problem for quantum systems. To formulate a feasible control objective, let $\lambda_\nu \in \mathbb{R}$ and $|\nu\rangle \in \mathbb{S}$ be an eigenvalue/eigenvector pair of H_0. Given the initial condition $|\psi(0)\rangle = e^{i\theta}|\nu\rangle$, with $\theta \in [0, 2\pi)$, system (8) admits the analytic solution

$$|\psi(t)\rangle = e^{i(\theta-\lambda_\nu t)}|\nu\rangle \tag{9}$$

which belongs to the (invariant) periodic orbit

$$\mathcal{O}_\nu = \{|\psi\rangle = e^{i\theta}|\nu\rangle \,|\, \theta \in [0, 2\pi)\}. \tag{10}$$

Geometrically, note that if $\mathbb{S}$ is a hypersphere in a $(4N+2)$-dimensional space, each of the $2N+1$ periodic orbits $\mathcal{O}_\nu$ is a circle lying on $\mathbb{S}$. Since each periodic orbit is isolated from all of the other ones, a suitable control objective for quantum systems is *"Design u(t) such that a given periodic orbit $\mathcal{O}_\nu \subset \mathbb{S}$ is a globally asymptotically stable limit cycle."* To illustrate why this control objective is physically relevant, "Eigenstates of the Hamiltonian" analyzes the structure of the eigenvectors $|\nu\rangle$ and explains what it means to drive the system to an eigenstate.

CONTROL STRATEGIES

This section provides a side-by-side comparison of notable strategies for quantum control synthesis. Readers wishing to familiarize themselves with these methods can find a variety of working examples to run on the Quantum Toolbox in Python (QuTiP) open source software [28], [29], [30]. Because of the introductory nature of this article, the numerical simulations will only consider the ideal case where the model is perfectly known and the state vector is fully accessible. Unfortunately, acquiring real-time measurements to perform quantum feedback control is generally not a trivial task [31], [32], [33], [34], [35], [36] since the very act of measuring the system inevitably introduces modifications to the state [35], [36]. Nevertheless, given sufficiently accurate models and/or suitable correction methods, the control strategies described in this article have been shown to produce satisfactory results when implemented in a predominantly open-loop fashion because of the high repeatability of quantum experiments. This includes Lyapunov-based control [37], [38], [39], [40], optimization-based control [41], [42], [43], [44], and learning-based control [45], [46], [47], [48].

Lyapunov Control

Lyapunov-based control design provides a relatively straightforward framework for obtaining an analytical feedback law [49], [50]. The principle behind this method is to choose an appropriate Lyapunov function candidate $V(\psi)$ and enforce $\dot{V}(\psi) < 0$ by defining a suitable control law $u(\psi)$. For an overview of Lyapunov-based control of quantum systems, the reader is referred to [51], [52], [53], [54], [55], and [56], which provide several alternative options for $V(\psi)$ and derive the resulting $u(\psi)$ for the case of bilinear systems. This article is limited to the Hilbert–Schmidt distance between the state $|\psi\rangle$ and a target eigenvector $|\nu\rangle$, that is,

$$V(\psi) = 1 - \langle\psi|\Pi_\nu|\psi\rangle. \tag{11}$$

To verify that (11) is a Lyapunov candidate function, note that the following hold, given $|\nu\rangle \in \mathbb{S}$ satisfying $H_0|\nu\rangle = \lambda_\nu|\nu\rangle$:

1) $\langle\psi|\Pi_\nu|\psi\rangle \in [0, 1]$, $\forall \psi \in \mathbb{S}$;
2) $\langle\psi|\Pi_\nu|\psi\rangle = 1 \Leftrightarrow \psi \in \mathcal{O}_\nu$, with $\mathcal{O}_\nu \subset \mathbb{S}$ satisfying (10).

Noting that $\langle\psi|\Pi_\nu|\psi\rangle = \langle\psi|\nu\rangle\langle\nu|\psi\rangle$, the time derivative of the Lyapunov candidate function is

$$\dot{V} = -\left(\frac{d\langle\psi|\nu\rangle}{dt}\langle\nu|\psi\rangle + \langle\nu|\psi\rangle\frac{d\langle\psi|\nu\rangle}{dt}\right).$$

Given the bilinear dynamic model (7), compute

$$\begin{aligned}\frac{d}{dt}\langle\nu|\psi\rangle &= \langle\nu|\dot{\psi}\rangle = \langle\nu|-i(H_0 + uH_1)\psi\rangle \\ &= -i\langle\nu|H_0|\psi\rangle - iu\langle\nu|H_1|\psi\rangle, \\ \frac{d}{dt}\langle\psi|\nu\rangle &= \langle\dot{\psi}|\nu\rangle = \langle -i(H_0 + uH_1)\psi|\nu\rangle \\ &= i\langle\psi|H_0|\nu\rangle + iu\langle\psi|H_1|\nu\rangle.\end{aligned}$$

Acquiring real-time measurements to perform quantum feedback control is generally not a trivial task since the very act of measuring the system inevitably introduces modifications to the state.

Since $|n\rangle$ is an eigenvector, we have $\langle\nu|H_0|\psi\rangle = \lambda_f\langle\nu|\psi\rangle$, leading to

$$\begin{aligned}\dot{V} &= i(\lambda_f\langle\nu|\psi\rangle + u\langle\nu|H_1|\psi\rangle)\langle\psi|\nu\rangle - i\langle\nu|\psi\rangle \\ &\quad\times(\lambda_f\langle\psi|\nu\rangle + u\langle\psi|H_1|\nu\rangle) \\ &= i\lambda_f|\langle\nu|\psi\rangle|^2 + iu\langle\nu|H_1|\psi\rangle\langle\psi|\nu\rangle - i\lambda_f|\langle\nu|\psi\rangle|^2 \\ &\quad - iu\langle\nu|\psi\rangle\langle\psi|H_1|\nu\rangle.\end{aligned}$$

Noting that $\langle\nu|\psi\rangle\langle\psi|H_1|\nu\rangle = (\langle\nu|H_1|\psi\rangle\langle\psi|\nu\rangle)^*$ and that $i(a-a^*) = -2\,\mathrm{Im}(a)$, the time derivative of the Lyapunov candidate function finally becomes

$$\dot{V} = -u\,2\,\mathrm{Im}(\langle\nu|H_1|\psi\rangle\langle\psi|\nu\rangle) \tag{12}$$

which can be made negative semidefinite by choosing the control law

$$u = \kappa\,\mathrm{Im}(\langle\nu|H_1|\psi\rangle\, e^{i\angle\langle\psi|\nu\rangle}) \tag{13}$$

where $\kappa > 0$ is a tuning parameter and $\angle a$ is the angle of the complex number a. With some abuse of notation, it is common to assign $\angle 0 = 0$ to prevent u from being undefined when $\langle\psi|\nu\rangle = 0$. As detailed in [57] and [58], it would be possible to prove that $\mathcal{O}_\nu$ is a globally asymptotically stable limit cycle if $\langle\nu|H_1|\psi\rangle \neq 0, \forall|\psi\rangle \in \mathbb{S}\backslash\mathcal{O}_\nu$. Unfortunately, this system does not satisfy this requirement. Indeed, it follows from (S11) that H_1 structurally ensures the following:

- If $|\psi\rangle$ is an *even* vector, $H_1|\psi\rangle$ is an *odd* vector.
- If $|\psi\rangle$ is an *odd* vector, $H_1|\psi\rangle$ is an *even* vector.

A $\mathbb{C}^{2N+1}$ vector is even (odd) if its ith element is equal (opposite) to its $2(N+1)-i$-th element for $i \in \{1, \ldots, N+1\}$. As discussed in "Eigenstates of the Hamiltonian," the target eigenvector $|\nu\rangle$ is either odd or even. Given that the inner product between odd and even vectors is always zero, we note that $\langle\nu|H_1|\psi\rangle = 0, \forall|\psi\rangle \in \Omega$, where Ω is the set of all odd (or even) unit vectors if $|\nu\rangle$ is odd (or even). Due to the fact that $\mathcal{O}_n \subset \Omega$, the proposed Lyapunov control law is formally unable to achieve the desired objectives. As shown in Figure 1, however, it is nevertheless possible to achieve a satisfactory transition from an even eigenstate to an odd eigenstate (and vice versa) given a properly chosen control gain $\kappa > 0$. Further improvements to the overall performance can be

Real Vector Representation

A typical assumption in the systems and control literature is that the state belongs to a real vector space. Indeed, a surprising number of numerical solvers and toolboxes implicitly rely on this assumption. Thus, it may be useful to know how to redefine a complex-valued wave function as real state vectors. Given $|\psi\rangle \in \mathbb{C}^n$, consider the bijective mapping

$$x = \begin{bmatrix}\mathrm{Re}(|\psi\rangle) \\ \mathrm{Im}(|\psi\rangle)\end{bmatrix}|\psi\rangle = [I_n \;\; 0]x + i[0 \;\; I_n]x \tag{S14}$$

where $x \in \mathbb{R}^{2n}$ is the new state vector and I_n is the identity matrix of size n. With no loss of generality, it can then be shown that the complex ordinary differential equation (ODE)

$$i\,|\dot{\psi}\rangle = H(u)\,|\psi\rangle \tag{S15}$$

which is equivalent to $|\dot{\psi}\rangle = -iH(u)\,|\psi\rangle$, can be rewritten as the real ODE

$$\dot{x} = \mathcal{J}\mathcal{H}(u)x \tag{S16}$$

where

$$\mathcal{J} = \begin{bmatrix}0 & I_n \\ -I_n & 0\end{bmatrix}, \quad \mathcal{H}(u) = \begin{bmatrix}\mathrm{Re}(H(u)) & -\mathrm{Im}(H(u)) \\ \mathrm{Im}(H(u)) & \mathrm{Re}(H(u))\end{bmatrix}.$$

Likewise, the quadratic form $\langle\psi|P|\psi\rangle$ admits the real vector equivalency

$$x^T\mathcal{P}\,x = \langle\psi\,|\,P\,|\,\psi\rangle \tag{S17}$$

with

$$\mathcal{P} = \begin{bmatrix}\mathrm{Re}(P) & -\mathrm{Im}(P) \\ \mathrm{Im}(P) & \mathrm{Re}(P)\end{bmatrix}. \tag{S18}$$

This bijective mapping allows us to, for example, reformulate the optimal control problem (15) using real-valued functions as follows:

$$\begin{aligned}&\text{minimize:} \quad x(T)^T\mathcal{P}\,x(T) + \int_0^T \eta(t)u^2(t)\,dt \\ &\text{subject to:} \quad \dot{x} = \mathcal{J}(\mathcal{H}_0 + \sin(u(t))\mathcal{H}_1 + (\cos(u(t)) - 1)\mathcal{H}_2)x(t), \\ &\qquad\qquad \forall t \in [0, T]\end{aligned} \tag{S19}$$

which extends the range of numerical tools that can be used to solve the optimization problem and/or simulate the behavior of the closed-loop system.

Because of the nonconvex nature of quantum optimal control problems, it should be noted that most solutions obtained with numerical solvers are local optima.

achieved by choosing a different Lyapunov function and/or introducing slight modifications to (13). Interested readers can find possible alternatives in [52], [53], [54], [55], and [56], although it should be noted that the existence of the invariant set Ω is a structural property of the control Hamiltonian H_1.

Optimal Control

Optimization-based control design provides a systematic framework for achieving high performance [59]. The principle behind this method is to find the trajectory $(\psi(t), u(t))$ that minimizes (or maximizes) an appropriate cost (or reward) function $J(\psi(t), u(t))$. For an overview of optimization-based control of quantum systems, readers are referred to [60], [61], and [62], which detail and compare existing numerical solvers (most of which are classified as either Krotov methods [63], [64] or gradient ascent pulse engineering methods [65]). "Real Vector Representation" illustrates how a quantum optimal control problem can be reformulated as a traditional (that is, real-valued) optimal control problem to enable the use of general-purpose trajectory optimization methods, such as the ones found in [66] and [67]. Because of the nonconvex nature of quantum optimal control problems, it should be noted that most solutions obtained with numerical solvers are local optima. This article considers the quantum optimal control problem

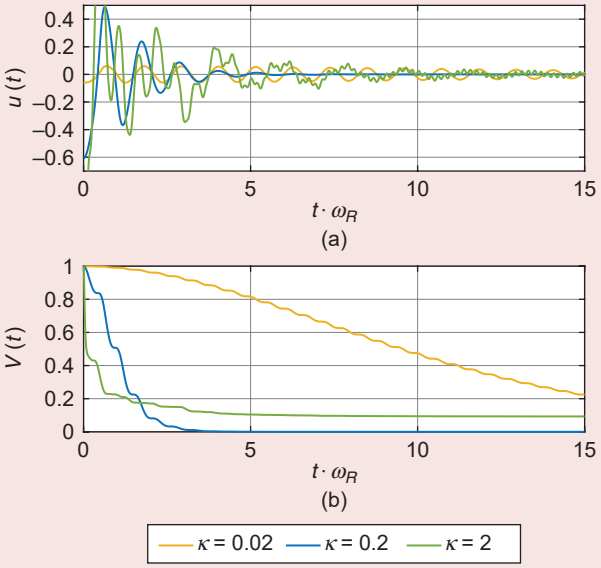

	$\kappa = 0.02$	$\kappa = 0.2$	$\kappa = 2$
$\lim_{t\to\infty} V(t)$	$9.2 \cdot 10^{-6}$	$6.1 \cdot 10^{-5}$	$9 \cdot 10^{-2}$
$t_{90\%}$	$20\ \omega_R^{-1}$	$1.9\ \omega_R^{-1}$	$1.4\ \omega_R^{-1}$

FIGURE 1 The behavior of (a) the control input and (b) the squared Hilbert–Schmidt distance obtained using the Lyapunov-based controller for three different values of the control gain κ. The choice of κ is subject to a tradeoff between two opposing performance parameters. On the one hand, lower gains are preferable because they lead to a smaller value of the final Hilbert–Schmidt distance [that is, $\lim_{t\to\infty} V(t)$]. On the other hand, higher gains are preferable because they entail a faster convergence [that is, $t_{90\%}$, which is the time at which V(t) reaches 90% of its final value].

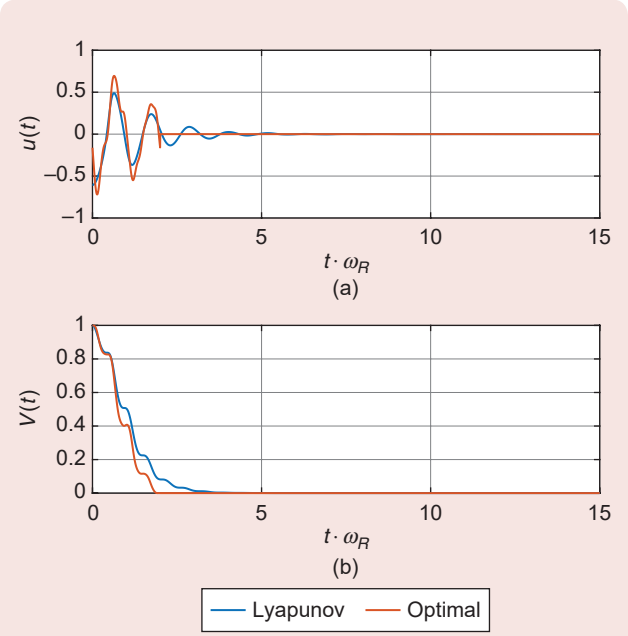

	Optimal	Lyapunov
$\lim_{t\to\infty} V(t)$	$1.6 \cdot 10^{-5}$	$6.1 \cdot 10^{-5}$
$t_{90\%}$	$1.63\ \omega_R^{-1}$	$1.9\ \omega_R^{-1}$

FIGURE 2 The behavior of (a) the control input and (b) the squared Hilbert–Schmidt distance obtained using the Lyapunov controller ($\kappa = 0.2$) and the optimal controller [$\eta(t) = 0.01$, and $T = 2$]. The optimal controller is able to outperform the Lyapunov controller by taking advantage of the fact that V(t) does not have to be a monotonically decreasing function.

Learning-based control is particularly effective in quantum applications due to the fact that all local minima are often associated with an equally satisfactory solution.

$$\begin{aligned}&\text{minimize: } \langle\psi(T)|P|\psi(T)\rangle + \int_0^T \eta(t)u^2(t)dt\\ &\text{subject to: } i|\dot{\psi}(t)\rangle = (H_0 + u(t)H_1)|\psi(t)\rangle, \quad \forall t \in [0,T] \end{aligned} \tag{14}$$

where $P = (I - \Pi_v)$ is the terminal cost matrix and $\eta(t) > 0$, $\forall t \in [0, T]$ is a tuning parameter. The optimization problem (14) can be interpreted as: *"Minimize the squared Hilbert–Schmidt distance between $|\psi(T)\rangle$ and the eigenvector $|v\rangle$, while also limiting the control effort."* In this article, the solution is computed using the approach detailed in [68]. For consistency with the Lyapunov-based controller, it is worth noting that (11), coupled with $\langle\psi|\psi\rangle = 1$, implies $\langle\psi|P|\psi\rangle = V(\psi)$. It is therefore possible to perform direct comparisons between the two control approaches by examining the behavior of $V(\psi(t))$. Figure 2 compares the performance of the Lyapunov-based controller with that of the optimization-based controller. Unsurprisingly, the latter achieves better performance in terms of both faster convergence and a more homogeneous use of the control input $u(t)$. It should also be noted that the optimal control framework enables dropping the small-angle approximation and working directly on the nonlinear dynamic model (6). This can be done by solving the quantum optimal control problem

$$\begin{aligned}&\text{minimize: } \langle\psi(T)|P|\psi(T)\rangle + \int_0^T \eta(t)u^2(t)dt\\ &\text{subject to: } i|\dot{\psi}(t)\rangle = (H_0 + \sin(u(t))H_1\\ &\qquad + (\cos(u(t)) - 1)H_2)|\psi(t)\rangle, \quad \forall t \in [0,T]. \end{aligned} \tag{15}$$

Figure 3 compares the response of the dynamic model (6), subject to the optimal control input obtained by solving (14) and (15). As expected, solving the optimal control problem on the bilinear model is not sufficient to ensure the convergence of the nonlinear model. This can be particularly problematic when doing an open-loop implementation of the control input.

Learning-Based Control

Learning-based control design provides a simple framework for generating model-agnostic control sequences. The principle behind this method is to define the control input $u(\theta, t)$ as a parameterized time-dependent function and use suitable learning strategies (for example, genetic algorithms [69] or the Nelder–Mead method [70]) to identify the parameter vector θ that minimizes a given cost function $f(\theta)$. As detailed in [71], learning-based control is particularly effective in quantum applications due to the fact that all local minima are often associated with an equally satisfactory solution. The most common input parameterization $u(\theta, t)$ is the chopped random basis (CRAB) method [72], [73], which defines the control input as a sum of sinusoids. Local minima that arise due to input constraints can be addressed using the dressed CRAB method [74]. Inspired by the CRAB formulation, this article defines the candidate control function as

$$u(\theta, t) = \mu(T_f, t)\sum_{k=1}^{K} a_k \sin(\omega_k t) + b_k \cos(\omega_k t) \tag{16}$$

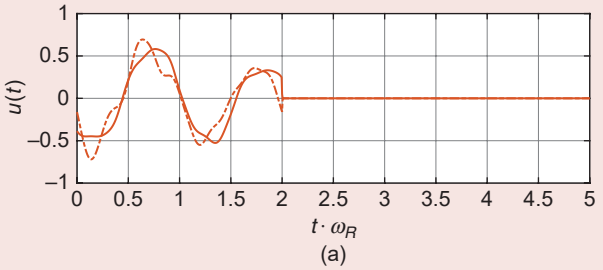

	Bilinear	Nonlinear
$\lim_{t\to\infty} V(t)$	$2.7 \cdot 10^{-2}$	$8.1 \cdot 10^{-6}$
$t_{90\%}$	1.65 ω_R^{-1}	1.7 ω_R^{-1}

FIGURE 3 A solution to (a) the bilinear (14) and nonlinear (15) optimal control problem and (b) the resulting behavior of the squared Hilbert–Schmidt distance obtained by simulating the response of the nonlinear model (6). In both cases, the optimization parameters were $\eta(t) = 0.01$, $\forall t \in [0, T]$, and $T = 2$. The comparison serves as a validation of the small-angle approximation used to obtain the bilinear model (7). Although the bilinear model (7) is pervasive in the existing quantum control literature, this figure shows that it can lead to performance degradation if the nonlinearities of the system are excited.

The Nelder–Mead Algorithm

The Nelder–Mead algorithm [S5] is a sampled gradient descent method for finding local minima in an $\mathbb{R}^N$ search space. To do so, first define a *simplex* as the convex hull of $N+1$ vertices. This is the simplest possible polytope that can be defined in $\mathbb{R}^N$ and reduces to a triangle in $\mathbb{R}^2$ and a tetrahedron in $\mathbb{R}^3$. Given a cost function $E(x)$ with $x \in \mathbb{R}^N$, the idea of the Nelder–Mead method is to evaluate $E(x)$ in each of the simplex vertices $\mathcal{S}^i = \{x_0^i, \ldots, x_N^i\}$ and then generate a new simplex $\mathcal{S}^{i+1}$ such that

$$\sum_{n=0}^{N} E(x_n^{i+1}) < \sum_{n=0}^{N} E(x_n^i). \tag{S20}$$

This is achieved by performing the following iteration rules:

1) Reorder the simplex vertices so that $E(x_0^i) \leq \ldots \leq E(x_N^i)$..
2) Compute the simplex centroid,

$$x_g^i = \frac{1}{N+1} \sum_{n=0}^{N} x_N^i. \tag{S21}$$

3) Compute the reflection of x_N^i with respect to the centroid,

$$x_r^i = x_g^i + (x_g^i - x_n^i). \tag{S22}$$

4) ***IF*** $\boldsymbol{E(x_0^i) < E(x_r^i) \leq E(x_{N-1}^i)}$**:**
   - Assign $x_n^{i+1} = x_n^i$ for $n = 0, \ldots, N-1$ and $x_N^{i+1} = x_r^i$;
   - Proceed to step 1) of the next iteration.

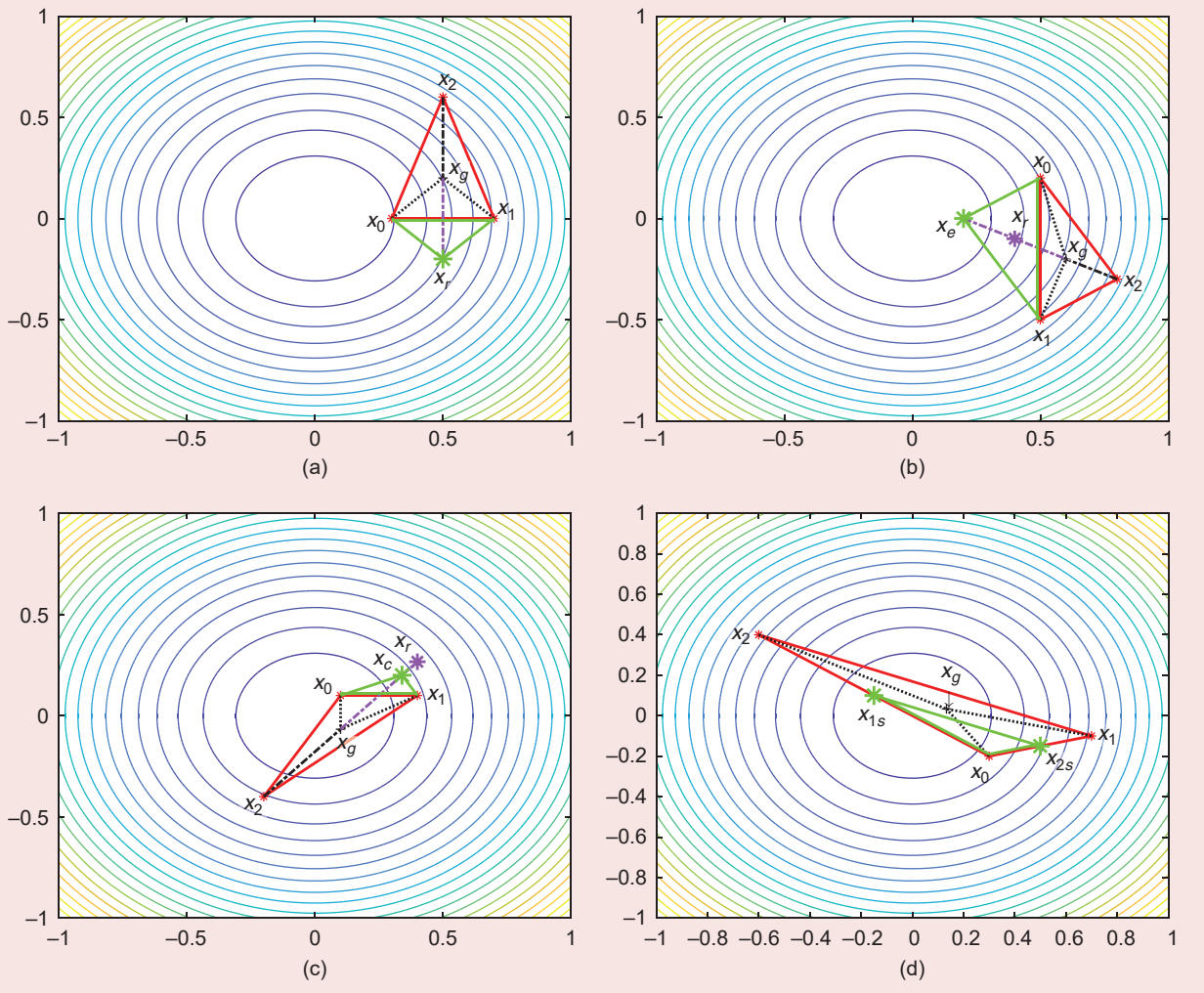

FIGURE S11 The Nelder–Mead algorithm is a sampled-data gradient descent method that iteratively generates a new simplex (green) with an average cost that is always lower than the previous simplex (red). Each subfigure represents a different operation of the algorithm given the cost function $E = \|x\|^2$, which is represented using contour lines. (a) *Reflect*: The point $x_r = x_g + (x_g - x_2)$ satisfies $E(x_0) < E(x_r) \leq E(x_1)$. Therefore, it is used as the vertex of the new simplex. (b) *Expand*: The point x_r satisfies $E(x_r) \leq E(x_0)$. Thus, the search is extended in the descent direction by computing $x_e = x_g + \gamma(x_g - x_2)$, with $\gamma > 1$. (c) *Contract*: Since $E(x_r) \geq E(x_2)$, a point is sought that is closer to the center of mass by computing $x_c = x_g + \rho(x_g - x_2)$, with $\rho \in (0, 1)$. However, it is only accepted if $E(x_c) < E(x_1)$. (d) *Shrink*: If all other conditions are not met, the simplex is too big to provide an accurate estimate of the gradient. Thus, the size is shrunk by fixing x_0 and computing x_{1s}, x_{2s} along the connectors with x_1, x_2.

5) *IF* $E(x_r^i) \leq E(x_0^i)$:

- Compute the expansion

$$x_e^i = x_g^i + \gamma(x_g^i - x_N^i), \quad \gamma > 1 \tag{S23}$$

- Assign $x_n^{i+1} = x_n^i$ for $n = 0, \ldots, N-1$ and $x_N^{i+1} = \text{argmin}\{E(x_r^i), E(x_e^i)\}$;
- Proceed to step 1) of the next iteration.

6) *IF* $E(x_r^i) \geq E(x_N^i)$:

- Compute the contraction

$$x_c^i = x_g^i + \rho(x_g^i - x_N^i), \quad 0 < \rho < 1 \tag{S24}$$

- ***AND IF*** $E(x_c^i) < E(x_{N-1}^i)$:
- Assign $x_n^{i+1} = x_n^i$ for $n = 0, \ldots, N-1$ and $x_N^{i+1} = x_c^i$;
- Proceed to step 1) of the next iteration.

7) *ELSE*: Shrink the entire simplex by computing

$$x_n^{i+1} = x_0^i + \sigma(x_n^i - x_0^i), \quad 0 < \sigma < 1. \tag{S25}$$

The iterative process ends when $\Sigma_{n=1}^{N} \| x_n^i - x_0^i \|^2 \leq \epsilon$, where $\epsilon > 0$ is a tolerance value. Intuitively, steps 4) through 6) seek to relocate the vertex with the highest cost (meaning x_N^i) somewhere along the line that connects x_N^i to the centroid x_g^i. If no suitable update is found, the simplex may be too large to provide a local estimate of the descent direction, which is why point 7) shrinks the simplex to improve the accuracy. The process ends when the maximum distance between all of the vertices is smaller than a given threshold, which signifies that the simplex has shrunk to a local minimum. Conceptual realizations of the Nelder–Mead algorithm applied in $\mathbb{R}^2$ are illustrated in Figure S11.

REFERENCE

[S5] J. A. Nelder and R. Mead, "A simplex method for function minimization," *Comput. J.*, vol. 7, no. 4, pp. 308–313, Jan. 1965, doi: 10.1093/comjnl/7.4.308.

where $\mu(T_f, t)$ is an envelope function, and the parameters are $\theta = [T_f, a_k, b_k, \omega_k]$, $k \in [1, \ldots, K]$. Clearly, the number of sinusoids K must be selected based on a tradeoff between computational complexity and the desired accuracy of the final solution. Fortunately, the model addressed in this article is such that the transition from the first eigenstate to the second can be achieved with only $K = 1$. Thus, the control input is

$$u(\theta, t) = \mu(T_f, t)(a \sin(\omega t) + b \cos(\omega t)) \tag{17}$$

and the envelope function is

$$\mu(T_f, t) = \begin{cases} \sin^2\left(\frac{\pi}{T_f} t\right) & \text{if } t \in [0, T_f] \\ 0 & \text{otherwise,} \end{cases} \tag{18}$$

which leads to a 4D parameter space $\theta = [T_f, a, b, \omega]$. Each control input estimate $u(\theta, t)$ is evaluated by integrating the system dynamics (6) to obtain $|\psi(\theta, t)\rangle$ and evaluating the Hilbert–Schmidt distance

$$f(\theta) = \langle \psi(\theta, T) | P | \psi(\theta, T) \rangle \tag{19}$$

where $P = (I - \Pi_v)$ and T is the time at which the measurement is taken (typically $T \geq T_f$ since the target is an eigenstate). "The Nelder–Mead Algorithm" details a systematic data-driven approach for finding a (locally) optimal set of parameters. Figure 4 compares the behavior obtained with the learning-based controller and the optimal controller obtained by solving (15). Note that the optimal controller used in this example features a time-varying input cost $\eta(t)$ chosen to mimic the behavior of the envelope function (18). Both laws were chosen to ensure a shaking function $u(t)$ with a smooth start and finish.

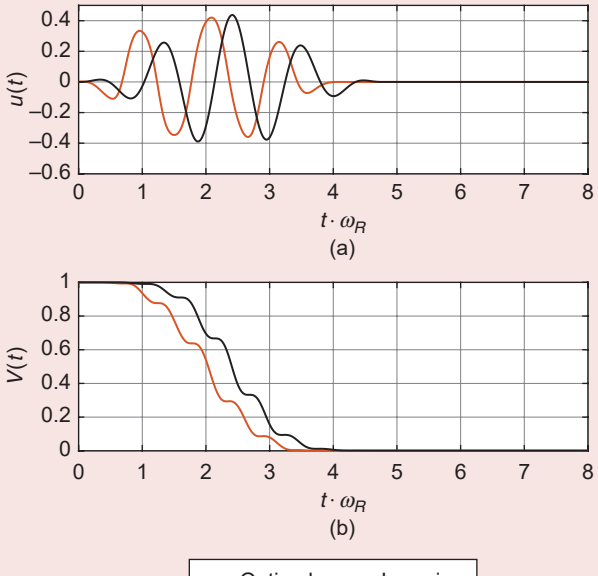

	Learning	Optimal
$\lim_{t\to\infty} V(t)$	$1.6 \cdot 10^{-3}$	$2.1 \cdot 10^{-6}$
$t_{90\%}$	$3.12\ \omega_R^{-1}$	$2.75\ \omega_R^{-1}$

FIGURE 4 The behavior of (a) the control input and (b) the squared Hilbert–Schmidt distance obtained using the optimal controller obtained by solving (15) (optimization parameters:

$$\eta(t) = \begin{cases} 0.01 \cdot 100^{T_1 - t} & \forall t \in [0, T_1) \\ 0.01 & \forall t \in [T_1, T_2] \\ 0.01 \cdot 100^{t - T_2} & \forall t \in (T_2, T] \end{cases}$$

$T_1 = 1, T_2 = 3$, and $T = 4$) and the learning-based controller (17) (learned parameters: $T_f = 4.7621$, $a = 0.1842$, $b = 0.3966$, and $\omega = 5.6762$). The two strategies perform similarly, with the optimal controller achieving a slightly better response (in terms of both faster settling time and lower control effort) and the learning-based controller having the advantage of being model agnostic.

CONCLUSIONS

This article offers a window onto a new and exciting field of control engineering. After introducing the fundamental postulates of quantum physics, the dynamic model of a BEC (that is, a cloud of ultracold atoms) trapped in an optical lattice is derived, and its dynamic behavior when the lattice is in its nominal configuration is analyzed. Using eigenvector decomposition, the physical interpretation of each eigenstate and what it means to transition from one eigenstate to another is discussed. Finally three different control strategies (Lyapunov based, optimization based, and learning based) for achieving said state-to-state transitions are introduced and compared. The article also serves as an invitation to all members of the IEEE Control Systems Society to not be discouraged by the perceived complexity of quantum physics and realize that this community has much to offer in terms of enabling the future directions of quantum technology.

ACKNOWLEDGMENT

The authors would like to acknowledge the University of Colorado Boulder CUbit initiative for enabling the formation of our multidisciplinary team of quantum physicists and control engineers. We would also like to acknowledge the National Science Foundation Quantum Idea Incubator for Transformational Advances in Quantum Systems for funding the team through award number 1936303. Marco M. Nicotra is the corresponding author.

AUTHOR INFORMATION

Marco M. Nicotra (marco.nicotra@colorado.edu) is with the University of Colorado Boulder, Boulder, CO 80309 USA.

Jieqiu Shao is with the University of Colorado Boulder, Boulder, CO 80309 USA.

Joshua Combes is with the University of Colorado Boulder, Boulder, CO 80309 USA.

Anne Cross Theurkauf is with the University of Colorado Boulder, Boulder, CO 80309 USA.

Penina Axelrad is with the University of Colorado Boulder, Boulder, CO 80309 USA.

Liang-Ying Chih is with the University of Colorado Boulder, Boulder, CO 80309 USA.

Murray Holland is with the University of Colorado Boulder, Boulder, CO 80309 USA.

Alex A. Zozulya is with Worcester Polytechnic Institute, Worcester, MA 01609 USA.

Catie K. LeDesma is with the University of Colorado Boulder, Boulder, CO 80309 USA.

Kendall Mehling is with the University of Colorado Boulder, Boulder, CO 80309 USA.

Dana Z. Anderson is with the University of Colorado Boulder, Boulder, CO 80309 USA.

REFERENCES

[1] T. Rosenband et al., "Frequency ratio of Al+ and Hg+ single-ion optical clocks; metrology at the 17th decimal place," *Science*, vol. 319, no. 5871, pp. 1808–1812, Mar. 2008, doi: 10.1126/science.1154622.

[2] S. Dimopoulos, P. W. Graham, J. M. Hogan, M. A. Kasevich, and S. Rajendran, "Gravitational wave detection with atom interferometry," *Phys. Lett. B*, vol. 678, no. 1, pp. 37–40, Jul. 2009, doi: 10.1016/j.physletb.2009.06.011.

[3] C. W. Chou, D. B. Hume, J. C. J. Koelemeij, D. J. Wineland, and T. Rosenband, "Frequency comparison of two high-accuracy Al+ optical clocks," *Phys. Rev. Lett.*, vol. 104, no. 7, Feb. 2010, Art. no. 070802, doi: 10.1103/PhysRevLett.104.070802.

[4] M. Hauth, C. Freier, V. Schkolnik, and A. Peters, "GAIN – A portable atom interferometer for on site measurements of local gravity," in *Frontiers in Optics*, P. Delyett Jr. and D. Gauthier, Eds. Washington, DC, USA: Optica Publishing Group, 2013.

[5] N. Gisin and R. Thew, "Quantum communication," *Nature Photon.*, vol. 1, no. 3, pp. 165–171, Mar. 2007, doi: 10.1038/nphoton.2007.22.

[6] L. Gyongyosi, S. Imre, and H. V. Nguyen, "A survey on quantum channel capacities," *IEEE Commun. Surveys Tuts.*, vol. 20, no. 2, pp. 1149–1205, Secondquarter 2018, doi: 10.1109/COMST.2017.2786748.

[7] P. P. Rohde, *The Quantum Internet: The Second Quantum Revolution*. Cambridge, U.K.: Cambridge Univ. Press, 2021.

[8] M. A. Nielsen and I. L. Chuang, *Quantum Computation and Quantum Information: 10th Anniversary Edition*. Cambridge, U.K.: Cambridge Univ. Press, 2010.

[9] L. Henriet et al., "Quantum computing with neutral atoms," *Quantum*, vol. 4, p. 327, Sep. 2020, doi: 10.22331/q-2020-09-21-327.

[10] P. Krantz, M. Kjaergaard, F. Yan, T. P. Orlando, S. Gustavsson, and W. D. Oliver, "A quantum engineer's guide to superconducting qubits," *Appl. Phys. Rev.*, vol. 6, no. 2, p. 021318, Jun. 2019, doi: 10.1063/1.5089550.

[11] D. Dong and I. R. Petersen, "Quantum control theory and applications: A survey," *IET Control Theory Appl.*, vol. 4, no. 12, pp. 2651–2671, Dec. 2010, doi: 10.1049/iet-cta.2009.0508.

[12] C. Brif, R. Chakrabarti, and H. Rabitz, "Control of quantum phenomena: Past, present and future," *New J. Phys.*, vol. 12, no. 7, Jul. 2010, Art. no. 075008, doi: 10.1088/1367-2630/12/7/075008.

[13] C. Altifani and F. Ticozzi, "Modeling and control of quantum systems: An introduction," *IEEE Trans. Autom. Control*, vol. 57, no. 8, pp. 1898–1917, Aug. 2012, doi: 10.1109/TAC.2012.2195830.

[14] Y.-J. Wang et al., "Atom Michelson interferometer on a chip using a Bose-Einstein condensate," *Phys. Rev. Lett.*, vol. 94, no. 9, Mar. 2005, Art. no. 090405, doi: 10.1103/PhysRevLett.94.090405.

[15] H. Müntinga et al., "Interferometry with Bose-Einstein condensates in microgravity," *Phys. Rev. Lett.*, vol. 110, no. 9, Feb. 2013, Art. no. 093602, doi: 10.1103/PhysRevLett.110.093602.

[16] T. Berrada, S. van Frank, R. Bücker, T. Schumm, J. Schaff, and J. Schmiedmayer, "Atom-interferometry constraints on dark energy," *Nature Commun.*, vol. 4, no. 1, p. 2077, Aug. 2015, doi: 10.1038/ncomms3077.

[17] C. A. Weidner, H. Yu, R. Kosloff, and D. Z. Anderson, "Robust calibration of an optical-lattice depth based on a phase shift," *Phys. Rev. A*, vol. 95, no. 4, Apr. 2017, Art. no. 043624, doi: 10.1103/PhysRevA.95.043624.

[18] C. N. Weiler, T. W. Neely, D. R. Scherer, A. S. Bradley, M. J. Davis, and B. P. Anderson, "Spontaneous vortices in the formation of Bose–Einstein condensates," *Nature*, vol. 455, no. 7215, pp. 948–951, Oct. 2008, doi: 10.1038/nature07334.

[19] S. Donadello et al., "Observation of solitonic vortices in Bose-Einstein condensates," *Phys. Rev. Lett.*, vol. 113, no. 6, Aug. 2014, Art. no. 065302, doi: 10.1103/PhysRevLett.113.065302.

[20] P.-E. Larré, A. Recati, I. Carusotto, and N. Pavloff, "Quantum fluctuations around black hole horizons in Bose-Einstein condensates," *Phys. Rev. A*, vol. 85, no. 1, Jan. 2012, Art. no. 013621, doi: 10.1103/PhysRevA.85.013621.

[21] F. Kühnel, "Bose-Einstein condensates with derivative and long-range interactions as set-ups for analog black holes," *Phys. Rev. D*, vol. 90, no. 8, Oct. 2014, Art. no. 084024, doi: 10.1103/PhysRevD.90.084024.

[22] P.-H. Chavanis, *Self-Gravitating Bose-Einstein Condensates*. New York, NY, USA: Springer-Verlag, 2015.

[23] T. E. Judd et al., "Zone-plate focusing of Bose–Einstein condensates for atom optics and erasable high-speed lithography of quantum electronic components," *New J. Phys.*, vol. 12, no. 6, Jun. 2010, Art. no. 063033, doi: 10.1088/1367-2630/12/6/063033.

[24] M. F. Fouda, R. Fang, J. B. Ketterson, and M. S. Shahriar, "Generation of arbitrary lithographic patterns using Bose-Einstein-condensate interferometry,"

Phys. Rev. A, vol. 94, no. 6, Dec. 2016, Art. no. 063644, doi: 10.1103/PhysRevA.94.063644.
[25] D. McIntyre, C. A. Manogue, and J. Tate, *Quantum Mechanics*. London, U.K.: Pearson Education, 2013.
[26] C. Cabrera-Gutiérrez et al., "Robust calibration of an optical-lattice depth based on a phase shift," *Phys. Rev. A*, vol. 97, no. 4, Apr. 2018, Art. no. 043617, doi: 10.1103/PhysRevA.97.043617.
[27] A. H. De Ruiter, C. J. Damaren, and J. R. Forbes, *Spacecraft Dynamics and Control: An Introduction*. Hoboken, NJ, USA: Wiley, 2013.
[28] J. R. Johansson, P. D. Nation, and F. Nori, "QuTiP: An open-source Python framework for the dynamics of open quantum systems," *Comput. Phys. Commun.*, vol. 183, no. 8, pp. 1760–1772, Aug. 2012, doi: 10.1016/j.cpc.2012.02.021.
[29] J. R. Johansson, P. D. Nation, and F. Nori, "QuTiP 2: A Python framework for the dynamics of open quantum systems," *Comput. Phys. Commun.*, vol. 184, no. 4, pp. 1234–1240, Apr. 2013, doi: 10.1016/j.cpc.2012.11.019.
[30] M. H. Goerz et al., "Krotov: A Python implementation of Krotov's method for quantum optimal control," *SciPost Phys.*, vol. 7, no. 6, p. 80, Dec. 2019, doi: 10.21468/SciPostPhys.7.6.080.
[31] A. N. Korotkov, "Selective quantum evolution of a qubit state due to continuous measurement," *Phys. Rev. B*, vol. 63, no. 11, Feb. 2001, Art. no. 115403, doi: 10.1103/PhysRevB.63.115403.
[32] L. Bouten, R. van Handel, and M. R. James, "A discrete invitation to quantum filtering and feedback control," *SIAM Rev.*, vol. 51, no. 2, pp. 239–316, May 2009, doi: 10.1137/060671504.
[33] L. Bouten, R. Van Handel, and M. R. James, "An introduction to quantum filtering," *SIAM J. Control Optim.*, vol. 46, no. 6, pp. 2199–2241, 2007, doi: 10.1137/060651239.
[34] K. Jacobs and D. A. Steck, "A straightforward introduction to continuous quantum measurement," *Contemporary Phys.*, vol. 47, no. 5, pp. 279–303, Sep. 2006, doi: 10.1080/00107510601101934.
[35] H. M. Wiseman and G. J. Milburn, *Quantum Measurement and Control*. Cambridge, U.K.: Cambridge Univ. Press, 2009.
[36] J. Zhang, Y.-x. Liu, R.-B. Wu, K. Jacobs, and F. Nori, "Quantum feedback: Theory, experiments, and applications," *Phys. Rep.*, vol. 679, pp. 1–60, Mar. 2017, doi: 10.1016/j.physrep.2017.02.003.
[37] Y. Zeng, T. Gebremariam, M. Ding, and C. Li, "Quantum optical diode based on Lyapunov control in a superconducting system," *J. Opt. Soc. Amer. B*, vol. 35, no. 9, pp. 2334–2341, Sep. 2018, doi: 10.1364/JOSAB.35.002334.
[38] Y. Ji, J. Hu, and Q. Ke, "Lyapunov-based states transfer for open system with superconducting qubits," *Int. J. Control, Automat. Syst.*, vol. 16, no. 1, pp. 55–61, Feb. 2018, doi: 10.1007/s12555-016-0069-8.
[39] C. Li, J. Song, Y. Xia, and W. Ding, "Driving many distant atoms into high-fidelity steady state entanglement via Lyapunov control," *Opt. Exp.*, vol. 26, no. 2, pp. 951–962, Jan. 2018, doi: 10.1364/OE.26.000951.
[40] D. Ran, W. Shan, Z. Shi, Z. Yang, J. Song, and Y. Xia, "High fidelity Dicke-state generation with Lyapunov control in circuit QED system," *Ann. Phys.*, vol. 396, pp. 44–55, Sep. 2018, doi: 10.1016/j.aop.2018.07.005.
[41] C. Lovecchio et al., "Optimal preparation of quantum states on an atom-chip device," *Phys. Rev. A*, vol. 93, Jan. 2016, Art. no. 010304, doi: 10.1103/PhysRevA.93.010304.
[42] S. van Frank et al., "Optimal control of complex atomic quantum systems," *Sci. Rep.*, vol. 6, no. 1, Oct. 2016, Art. no. 34187, doi: 10.1038/srep34187.
[43] R. W. Heeres, P. Reinhold, N. Ofek, L. J. L. Frunzio, M. H. Devoret, and R. J. Schoelkopf, "Implementing a universal gate set on a logical qubit encoded in an oscillator," *Nature Commun.*, vol. 8, no. 1, Jul. 2017, Art. no. 94, doi: 10.1038/s41467-017-00045-1.
[44] G. Feng et al., "Gradient-based closed-loop quantum optimal control in a solid-state two-qubit system," *Phys. Rev. A*, vol. 98, no. 5, Nov. 2018, Art. no. 052341, doi: 10.1103/PhysRevA.98.052341.
[45] S. Rosi et al., "Fast closed-loop optimal control of ultracold atoms in an optical lattice," *Phys. Rev. A*, vol. 88, no. 2, Aug. 2013, Art. no. 021601, doi: 10.1103/PhysRevA.88.021601.
[46] V. C. Gregoric, X. Kang, Z. C. Liu, Z. A. Rowley, T. J. Carroll, and M. W. Noel, "Quantum control via a genetic algorithm of the field ionization pathway of a Rydberg electron," *Phys. Rev. A*, vol. 96, no. 2, Aug. 2017, Art. no. 023403, doi: 10.1103/PhysRevA.96.023403.
[47] F. Frank et al., "Autonomous calibration of single spin qubit operations," *NPJ Quantum Inf.*, vol. 3, no. 1, Dec. 2017, Art. no. 48, doi: 10.1038/s41534-017-0049-8.
[48] C. A. Weidner, H. Yu, R. Kosloff, and D. Z. Anderson, "Experimental demonstration of shaken-lattice interferometry," *Phys. Rev. Lett.*, vol. 120, no. 26, Jun. 2018, Art. no. 263201, doi: 10.1103/PhysRevLett.120.263201.
[49] A. Isidori, *Nonlinear Control Systems*. New York, NY, USA: Springer-Verlag, 1995.
[50] H. K. Khalil, *Nonlinear Systems*, 3rd ed. Englewood Cliffs, NJ, USA: Prentice-Hall, 2002.
[51] S. Grivopoulos and B. Bamieh, "Lyapunov-based control of quantum systems," in *Proc. 42nd IEEE Int. Conf. Decis. Control (IEEE Cat. No. 03CH37475)*, 2003, vol. 1, pp. 434–438, doi: 10.1109/CDC.2003.1272601.
[52] M. Mirrahimi, P. Rouchon, and G. Turinici, "Lyapunov control of bilinear Schrödinger equations," *Automatica*, vol. 41, no. 11, pp. 1987–1994, Nov. 2005, doi: 10.1016/j.automatica.2005.05.018.
[53] S. Kuang and S. Cong, "Lyapunov control methods of closed quantum systems," *Automatica*, vol. 44, no. 1, pp. 98–108, Jan. 2008, doi: 10.1016/j.automatica.2007.05.013.
[54] X. Wang and S. G. Schirmer, "Analysis of Lyapunov method for control of quantum states," *IEEE Trans. Autom. Control*, vol. 55, no. 10, pp. 2259–2270, Oct. 2010, doi: 10.1109/TAC.2010.2043292.
[55] S. Cong and F. Meng, "A survey of quantum Lyapunov control methods," *Sci. World J.*, vol. 2013, May 2013, Art. no. 967529, doi: 10.1155/2013/967529.
[56] S. Kuang, D. Dong, and I. R. Petersen, "Rapid Lyapunov control of finite-dimensional quantum systems," *Automatica*, vol. 81, pp. 164–175, Jul. 2017, doi: 10.1016/j.automatica.2017.02.041.
[57] M. Mirrahimi and P. Rouchon, "Trajectory generation for quantum systems based on Lyapounov techniques," *IFAC Proc. Volumes*, vol. 37, no. 13, pp. 291–296, Sep. 2004, doi: 10.1016/S1474-6670(17)31238-7.
[58] S. Cong and S. Kuang, "Quantum control strategy based on state distance," *Acta Autom. Sinica*, vol. 33, no. 1, pp. 28–31, Jan. 2007, doi: 10.1360/aas-007-0028.
[59] D. E. Kirk, *Optimal Control Theory: An Introduction*. Englewood Cliffs, NJ, USA: Prentice-Hall, 1998.
[60] D. D'Alessandro, *Introduction to Quantum Control and Dynamics*. London, U.K.: Chapman & Hall, 2008.
[61] S. Machnes et al., "Comparing, optimizing, and benchmarking quantum-control algorithms in a unifying programming framework," *Phys. Rev. A*, vol. 84, no. 2, Aug. 2011, Art. no. 022305, doi: 10.1103/PhysRevA.84.022305.
[62] S. J. Glaser et al., "Training Schrödinger's cat: Quantum optimal control," *Eur. Phys. J. D*, vol. 69, Dec. 2015, Art. no. 279, doi: 10.1140/epjd/e2015-60464-1.
[63] V. F. Krotov and I. N. Feldman, "Iteration method of solving the problems of optimal control," *Eng. Cybern.*, vol. 21, no. 2, pp. 123–130, 1983.
[64] D. M. Reich, M. Ndong, and C. P. Koch, "Monotonically convergent optimization in quantum control using Krotov's method," *J. Chem. Phys.*, vol. 136, no. 10, p. 104,103, Mar. 2012, doi: 10.1063/1.3691827.
[65] N. Khaneja, T. Reiss, C. Kehletb, T. Schulte-Herbrüggen, and S. J. Glaser, "Optimal control of coupled spin dynamics: Design of NMR pulse sequences by gradient ascent algorithms," *J. Magn. Reson.*, vol. 172, no. 2, pp. 296–305, Feb. 2005, doi: 10.1016/j.jmr.2004.11.004.
[66] J. Hauser, "A projection operator approach to the optimization of trajectory functionals," *IFAC Proc. Volumes*, vol. 35, no. 1, pp. 377–382, Jan. 2002, doi: 10.3182/20020721-6-ES-1901.00312.
[67] D. Garg, M. Patterson, W. Hager, A. Rao, D. Benson, and G. Huntington, "A unified framework for the numerical solution of optimal control problems using pseudospectral methods," *Automatica*, vol. 46, no. 11, pp. 1843–1851, Nov. 2010, doi: 10.1016/j.automatica.2010.06.048.
[68] J. Shao, J. Combes, J. Hauser, and M. M. Nicotra, "Projection-operator-based Newton method for the trajectory optimization of closed quantum systems," *Phys. Rev. Lett. A*, vol. 105, Mar. 2022, Art. no. 032605, doi: 10.1103/PhysRevA.105.032605.
[69] D. A. Coley, *An Introduction to Genetic Algorithms for Scientists and Engineers*. River Edge, NJ, USA: World Scientific, 1999.
[70] J. Nelder and R. Mead, "A simplex method for function minimization," *Comput. J.*, vol. 7, no. 4, pp. 308–313, Jan. 1965, doi: 10.1093/comjnl/7.4.308.
[71] H. A. Rabitz, M. M. Hsieh, and C. M. Rosenthal, "Quantum optimally controlled transition landscapes," *Science*, vol. 303, no. 5666, pp. 1998–2001, Mar. 2004, doi: 10.1126/science.1093649.
[72] P. Doria, T. Calarco, and S. Montangero, "Optimal control technique for many-body quantum dynamics," *Phys. Rev. Lett.*, vol. 106, no. 19, May 2011, Art. no. 190501, doi: 10.1103/PhysRevLett.106.190501.
[73] T. Caneva, T. Calarco, and S. Montangero, "Chopped random-basis quantum optimization," *Phys. Rev. A*, vol. 84, no. 2, Aug. 2011, Art. no. 022326, doi: 10.1103/PhysRevA.84.022326.
[74] N. Rach, M. M. Müller, T. Calarco, and S. Montangero, "Dressing the chopped-random-basis optimization: A bandwidth-limited access to the trap-free landscape," *Phys. Rev. A*, vol. 92, no. 6, Dec. 2015, Art. no. 062343, doi: 10.1103/PhysRevA.92.062343.